Nanoscale

PAPER

View Article Online
View Journal | View Issue

Cite this: *Nanoscale*, 2017, **9**, 6755

Granular topological insulators†

Abhishek Banerjee,[a] Oindrila Deb,[b] Kunjalata Majhi,[a] R. Ganesan,[a] Diptiman Sen[b] and P. S. Anil Kumar *[a]

Received 23rd February 2017,
Accepted 23rd April 2017

DOI: 10.1039/c7nr01355h

rsc.li/nanoscale

We demonstrate experimentally that a macroscopic topological insulator (TI) phase can emerge in a granular conductor composed of an assembly of tunnel coupled TI nanocrystals of dimension ~10 nm × 10 nm × 2 nm. Electrical transport measurements on thin films of Bi_2Se_3 nanocrystals reveal the presence of decoupled top and bottom topological surface states that exhibit large surface state penetration depths (~30 nm at 2 K). By tuning the size of the nanocrystals and the couplings between them, this new class of TIs may be readily tuned from a non-topological to a topological insulator phase, that too with designer properties. Paradoxically, this seemingly 'dirty' system displays properties that are closer to an ideal TI than most known single crystal systems, making granular/nanocrystalline TIs an attractive platform for future TI research.

1. Introduction

Topological insulators (TIs) have recently emerged as an exciting class of materials that are insulating in the bulk and conduct electricity at the surface.[1,2] The surface conduction is supported by helical Dirac fermion states that are protected by the topology of the bulk band structure.[3–6] Such topological surface states (TSS) have been used to demonstrate a host of exotic phenomena including spin polarized current conduction,[7] quantum anomalous Hall effect,[8] Majorana bound states,[9] and high temperature quantum Hall effects.[10] However, demonstrations of TSS have until now been limited to single crystalline TI materials or thin films showing long-range order over several hundred nanometers.[11–13] The nanocrystalline regime of these materials remains completely unexplored, and it is not clear even theoretically whether the topological properties of TIs survive deformations down to the nanoscale regime. More interestingly, such non-continuous deformations of topological insulator systems have been theoretically predicted to give rise to more exotic emergent topological phases such as Weyl semimetals,[14] strong, weak and crystalline topological insulators in TI multilayers[15–17] and bulk topological proximity effects in coupled non-TI/TI heterostructures.[18] A distinctive feature of these topological systems is that band inversions are governed primarily by geometry apart from spin–orbit coupling, correlations[19] or disorder.[20] While the latter properties are difficult to manipulate in realistic materials, current nanofabrication technologies provide unprecedented control over sample geometry.[21,22] Therefore such systems can be used to fabricate designer/artificial topological insulators[15,17] where topological properties may be tuned by externally controllable parameters in easily accessible materials and their superlattices. Such control of topology could find immense applications in quantum information processing and spin-based electronic devices that rely on the topological protection of electronic states.

In this work, we consider a granular TI built out of an assembly of tunnel coupled Bi_2Se_3 nanocrystals (Fig. 1(a)). Granular TI thin films consisting of micron sized crystallites have been previously studied and shown to give rise to interesting phenomena such as disorder induced linear magnetoresis-

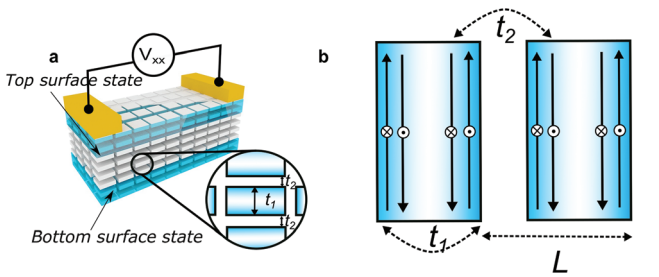

Fig. 1 (a) Schematic of a granular system composed of ordered TI granules. (b) shows tunnel coupled Dirac fermion states on the surfaces of TI nanocrystals. The cross and dot marks represent the spin polarizations of channels with opposite momenta. t_1 and t_2 are the tunneling amplitudes between intra-grain and inter-grain surfaces respectively.

[a]*Department of Physics, Indian Institute of Science, Bengaluru 560 012, India. E-mail: anil@physics.iisc.ernet.in*
[b]*Centre for High Energy Physics, Indian Institute of Science, Bengaluru 560 012, India*

†Electronic supplementary information (ESI) available. See DOI: 10.1039/C7NR01355H

tance,[11] high frequency photo-galvanic effect,[12] and anomalous photoelectric effects.[13] However the crystallite sizes in previous experiments were too large to induce any significant topological distinction from ideal single crystal TIs. On the other hand, the nanocrystalline regime we consider here has not been explored before. We demonstrate that under certain conditions, this coupled system indeed becomes a macroscopic TI hosting topological surface states. Moreover, we reveal several intriguing properties of this system that make it distinctly different and potentially more useful than all previously considered TIs.

2. Theoretical model

We first present a simple model of a granular TI where the low-energy properties are governed by interactions between the Dirac fermion states localized on the surfaces of individual nanocrystals; we ignore the bulk states of the individual nanocrystals as they are separated from the surface states by a gap. Guided by the experimental observations (described later) that the nanocrystalline grains are quite well-ordered along the c-axis (called the z-direction) and that the in-plane (x–y directions) grain size is much larger than the grain thickness, we consider a system consisting of a regular array of grains which are infinitely large in-plane (surface) and repeat periodically in the z-direction, with a unit cell size $L \sim 2$ nm (Fig. 2(a)). The effects of statistical variations of the grain sizes will be discussed later.

Labeling the top and bottom surfaces of the n-th grain as $(1, n)$ and $(3, n)$ respectively, the Dirac Hamiltonian governing the electrons on the surface $(1, n)$ is $H_1 = i\hbar v_F(\sigma^y\partial_x - \sigma^x\partial_y)$, and on the surface $(3, n)$ is $H_3 = i\hbar v_F(\sigma^y\partial_x - \sigma^x\partial_y)$, where v_F is the Fermi velocity on the x–y surface and is given by 0.333 eV nm/$\hbar$ for Bi_2Se_3,[23,24] and σ^a denotes the Pauli spin matrices. The translational invariance in the x and y directions allow us to label the states by the momentum $\vec{k} = (k_x, k_y)$ which has the same value in all the grains. Next we introduce an intra-grain tunneling t_1 between the opposite surfaces of the same grain, $(1, n)$ and $(3, n)$, and an inter-grain tunneling coupling t_2 between the nearby surfaces of neighbouring grains, $(3, n)$ and $(1, n + 1)$. For simplicity we will assume that the couplings t_1 and t_2 are both real and positive.

The couplings t_1 and t_2 can be experimentally controlled as follows. On increasing the temperature, the inter-grain coupling t_2 becomes stronger; this may be due to a combination of (i) thermally assisted tunneling through a barrier formed by the charging energies of the grains (namely, if two grains have N electrons each, the tunneling of an electron from one grain to the other changes the electron numbers to $N - 1$ and $N + 1$. This typically increases the total charging energy of the two grains by some energy ΔE; the associated tunneling probability $e^{-\Delta E/(k_B T)}$ increases with temperature), and (ii) the effective distance between the surfaces decreasing with increasing temperature, as is known to happen in some quantum Hall systems.[25] The intra-grain coupling t_1 does not change the charging energy of a grain and is therefore not expected to vary significantly with temperature. On the other hand, t_1 will depend strongly on the individual grain sizes. Increasing the size of a grain increases the distance between its opposite surfaces; this decreases the overlap of the surface states at the opposite surfaces of the grain and hence t_1 decreases.

Putting the Dirac Hamiltonians and the tunnelings together, we obtain an effectively one-dimensional model in which the unit cell n has two-component wave functions $\psi_{1,n}$ and $\psi_{3,n}$. The complete Hamiltonian takes the form

$$\begin{aligned} H = \sum_n \Big[& \psi_{1,n}^\dagger \hbar v_F(\sigma^x k_y - \sigma^y k_x)\psi_{1,n} \\ & - \psi_{3,n}^\dagger \hbar v_F(\sigma^x k_y - \sigma^y k_x)\psi_{3,n} \\ & + (t_1 \psi_{1,n}^\dagger \psi_{3,n} + t_2 \psi_{3,n}^\dagger \psi_{1,n+1} + \text{H.c.})\Big], \end{aligned} \tag{1}$$

where $(k_x k_y)$ is the momentum in the x–y directions.

If the number of grains is infinite, with n going from $-\infty$ to ∞, the Bloch momentum k_z is a good quantum number. We can then set $\psi_{1,n} = e^{ik_z L n}\alpha_1$ and $\psi_{3,n} = e^{ik_z L n}\alpha_3$, where α_1 and α_3 are two-component spinors and k_z lies in the range $[-\pi/L, \pi/L]$. We then obtain the equations

$$\begin{aligned} \hbar v_F(\sigma^x k_y - \sigma^y k_x)\alpha_1 + (t_1 + t_2 e^{-ik_z L})\alpha_3 &= E\alpha_1, \\ -\hbar v_F(\sigma^x k_y - \sigma^y k_x)\alpha_3 + (t_1 + t_2 e^{ik_z L})\alpha_1 &= E\alpha_3. \end{aligned} \tag{2}$$

This gives the energy spectrum

$$E_{\vec{k}\pm} = \pm\sqrt{\hbar^2 v_F^2 k^2 + t_1^2 + t_2^2 + 2t_1 t_2 \cos(k_z L)}, \tag{3}$$

where $k = \sqrt{k_x^2 + k_y^2}$. We see that the spectrum is gapped at $k_x = k_y = 0$, the gap being equal to $2|t_1 - t_2|$ at $k_z L = \pm\pi$. If we think of the entire system as a single object, these states can be called the 'bulk' states since the wave function is non-zero for all values of n.

Let us now consider a system with a finite number of grains, so that n goes from 1 to N. Assuming that $N \gg 1$, we look for 'surface' states whose wave functions are $\psi_{3,n} = (-1)^n e^{-nL/\lambda}\alpha_3$ exponentially localized near either $n = 1$ (the top surface) or $n = N$ (the bottom surface of the entire system). For states localized near $n = 1$ we discover that we have to take $\psi_{1,n} = (-1)^n e^{-nL/\lambda}\alpha_1$ and $\psi_{3,n} = (-1)^n e^{-nL/\lambda}\alpha_3$, where the decay length λ must be real and positive. This leads to the equations

$$\begin{aligned} \hbar v_F(\sigma^x k_y - \sigma^y k_x)\alpha_1 + (t_1 - t_2 e^{L/\lambda})\alpha_3 &= E\alpha_1, \\ -\hbar v_F(\sigma^x k_y - \sigma^y k_x)\alpha_3 + (t_1 - t_2 e^{-L/\lambda})\alpha_1 &= E\alpha_3. \end{aligned} \tag{4}$$

We then find there are solutions with $\alpha_3 = 0$, namely, $\psi_{3,n} = 0$, and

$$E_{\vec{k}\pm} = \pm\hbar v_F k \text{ and } e^{-L/\lambda} = \frac{t_1}{t_2}. \tag{5}$$

We see that surface states exist only if $t_1 < t_2$, so that $\lambda > 0$. Similarly, we find that there are states localized near $n = N$,

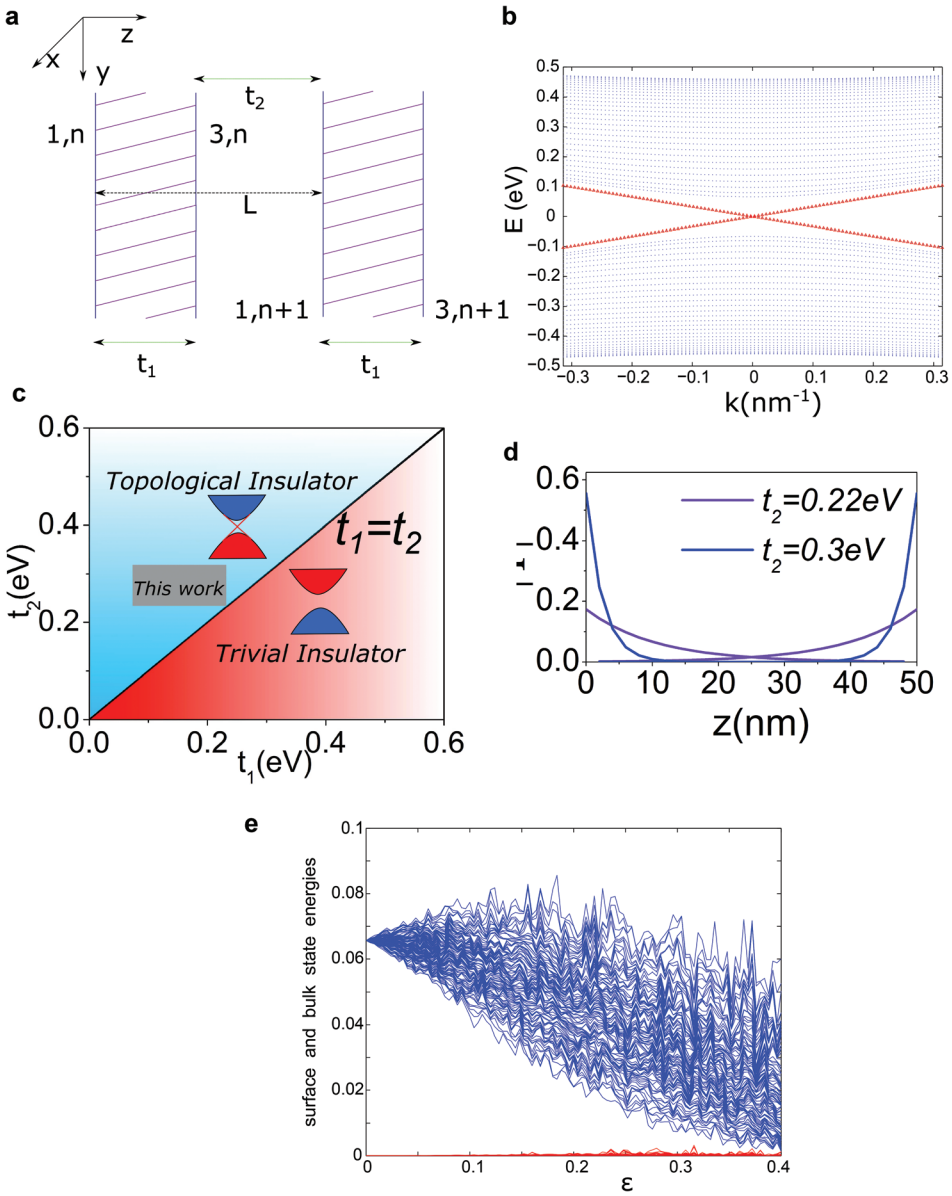

Fig. 2 (a) A system of TI grains with surfaces 1 and 3. All the surfaces extend infinitely in the x and y directions. The intra-grain coupling between surfaces (1, n) and (3, n) of the grain labeled n is t_1, while the inter-grain coupling between surfaces (3, n) and (1, $n + 1$) is t_2. The size of the unit cell in the z direction is L. (b) Energy dispersion with $N = 30$, $\nu_F = 0.333$ eV nm, $t_1 = 0.2$ eV, $t_2 = 0.26$ eV, and $-0.1\pi < k < 0.1\pi$ in nm^{-1}. Both bulk states (blue dots) and surface states (red triangles) are shown. (c) indicates that the interplay between t_1 and t_2 gives rise to a trivial insulator phase when $t_1 > t_2$ and a topological insulator phase when $t_2 > t_1$. (d) The probability density $|\Psi|^2$ shows the penetration of the top and bottom surface state wave functions into the bulk of the TI for two different values of t_2 at a constant value of $t_1 = 0.2$ eV. (e) Surface state energies (near zero energy in red) and the lowest bulk state energies (in the middle in blue) for $k = 0$ in a disordered system as a function of the strength ε of the disorder in the couplings t_1 and t_2; see the text for details.

with $\psi_{1N} = 0$, $\psi_{3,\,n} = (-1)^n e^{(n-N)L/\lambda}\alpha_3$, and E and λ are again given by eqn (5). The second equation in (5) shows that if t_1/t_2 is close to 1, a small change in t_2 (due to a change in temperature) can change λ by a large amount.

If the number of grains N is finite and not very large, then the surface states near $n = 1$ and $n = N$ will hybridize, thereby altering their energies from eqn (5). Let us introduce a pseudospin Pauli matrix s^z which has the value +1 for states near $n = 1$ and −1 for states near $n = N$. The hybridization between these two kinds of states will be described by the matrix s^x. Let γ be the hybridization amplitude; this will be a function of t_1, t_2 and N. We find that

$$\gamma \simeq t_2\left(1 - \frac{{t_1}^2}{{t_2}^2}\right)\left(\frac{t_1}{t_2}\right)^N \qquad (6)$$

if $(t_1/t_2)^N \ll 1$. The effective Hamiltonian describing the states at only the top and bottom surfaces is then given by

$$H = \hbar\nu_F(\sigma^x k_y - \sigma^y k_x)s^z + \gamma s^x. \quad (7)$$

The energy spectrum of this is given by

$$E_{\vec{k}\pm} = \pm\sqrt{\hbar^2\nu_F{}^2k^2 + \gamma^2}. \quad (8)$$

The value of γ can be found numerically by evaluating the spectrum of eqn (1) for $k_x = k_y = 0$ and some given values of t_1t_2 and N. The states which lie within the bulk gap will have the energies $\pm\gamma$; this enables us to read off the value of γ. The knowledge of γ then determines the Hamiltonian in eqn (7) completely.

In Fig. 2(b), we show all the energy levels as a function of k for a system with 30 grains, $t_1 = 0.2$ eV and $t_2 = 0.26$ eV. For a given value of k, eqn (3) shows that the energies of the bulk states (blue dots) lie in the range $\hbar^2\nu_F{}^2k^2 + (t_1 - t_2)^2 \le E^2 \le \hbar^2\nu_F{}^2k^2 + (t_1 + t_2)^2$, depending on the value of k_zL; at $k = 0$, the bulk states have a gap equal to $|t_1 - t_2|$. The surface states also have a gap at $k = 0$ given by the expression in eqn (6); however this is too small to see in the figure.

We conclude that there are surface states if $t_1 < t_2$ (therefore called a topological phase); then the system with many grains of TIs behave like a single TI with states at the top and bottom surfaces which have a linear dispersion. If $t_1 > t_2$ the system is in a non-topological phase. The bulk is gapped in both phases. The two phases are separated by a quantum critical line given by $t_1 = t_2$ where the bulk becomes gapless (Fig. 2(c)).

In experiments, the inter-grain tunneling t_2 can be changed by varying the temperature as discussed above. If t_1 is assumed to be constant, we see from eqn (5) and (6) that both the decay length λ of the surface states and the coupling γ between the end surfaces at $n = 1$ and $n = N$ decrease as t_2 increases (Fig. 2(d)). A remarkable consequence of this is that the surface state decay length can span over several grains, clearly manifesting the topological nature of the surface states. More importantly, this feature can be used to experimentally distinguish granular TIs from conventional crystalline TIs where the surface state penetration depths are significantly shorter and are non-tunable.

We end this section by discussing the effects of disorder on the existence of surface states. A remarkable feature of three-dimensional TIs is that weak non-magnetic disorder (which does not break time reversal symmetry) does not destroy the surface states.[2] We therefore expect the surface states to survive small variations in the sizes and shapes of the grains. We have studied this numerically as follows. In the system described in Fig. 2(a), we take the couplings to be of the form $(t_1)_{n,n} = (0.2 + \varepsilon r)$ eV and $(t_2)_{n,n+1} = (0.26 + \varepsilon r)$ eV, where each r is an independent random variable chosen from a uniform probability distribution in the range $[-0.5, 0.5]$, and ε denotes the strength of the disorder. For a given set of such randomly chosen t_1 and t_2, we compute all the energy levels for $k = 0$. These come in $\pm$ pairs (due to a sub-lattice symmetry of the Hamiltonian), and each energy has a double degeneracy due to spin. Among the positive energy states, we find that there are two surface states with the same energy E_0; we also find the two bulk states with the lowest energy E_1. We then consider 100 different realizations of randomness, thus giving us many values of E_0 and E_1. In Fig. 2(e), we have shown the central 96% of these 100 values (corresponding to a 2σ deviation from the mean) as a function of the disorder strength ε; the red lines appearing close to zero energy are E_0 while the blue lines appearing near the middle are E_1. We see that the surface and bulk states remain well-separated until at least $\varepsilon \sim 0.1$; we have checked that the states corresponding to energy E_0 remain localized near the top and bottom surfaces in all cases. We thus see that as long as the disorder strength is smaller than $|t_1 - t_2|$, so that $t_1 < t_2$ on the average, small variations in t_1 and t_2 for individual grains do not affect the presence of surface states lying inside the bulk gap.

3. Experiment

Thin films of Bi_2Se_3 nanocrystals are grown on high resistivity Si(111) substrates using pulsed laser deposition.[26] The degree of granularity in these films is controlled by tuning the laser pulse energy and is quantified using atomic force microscopy and X-ray diffraction (Fig. 3(a–c)). Our measurements indicate an in-plane crystalline coherence length $\xi_\parallel \approx 10$ nm, which is the same as the in-plane grain size. The vertical grain size is smaller and is estimated to be ~2–3 nm which sets the value of $t_1 \sim 0.1$–0.2 eV while t_2 is determined by the strength of van der Waals bonding in the c-axis direction. XRD and AFM measurements on all our samples show identical granular structures and grain sizes.[26]

To establish the presence of a TI phase in our samples, we need to demonstrate the presence of topological surface states. The highly granular nature of our nanocrystalline TI films precludes experiments like angle resolved photoemission spectroscopy (ARPES) or scanning tunneling microscopy that require a high degree of crystalline order. Therefore we turn to electrical conductance measurements to detect signatures of TI transport.

Electrical transport measurements are carried out on granular TI films with thickness ranging from 8 nm to 153 nm. The temperature dependence of the resistance shown in Fig. 3(d) reveals signatures that are typical of granular materials.[27] A strong insulating upturn is seen below ~30 K for $T \to 0$ K indicating a tendency towards Anderson localization. To probe this further, we use Hall effect measurements (at 2 K) to estimate the disorder introduced by granularity. We observe a linear Hall effect up to a maximum field of 7 T (Fig. 3(e)) indicating that electrical transport is dominated by a single carrier. The values of carrier density (n_{3D}) and mobility (μ) are shown in Fig. 3(f). For a typical sample, assuming a spherical Fermi surface we estimate a Fermi momentum $k_F = (3\pi^2 n_{3D})^{1/3} \sim 0.8$–$0.9$ nm^{-1} and a mean free path $l_e = (\hbar\mu/e)k_F \sim 2$–$3$ nm. The extent of disorder in our samples can be estimated by using the Ioffe–Regel criterion for which $g = k_F l_e \gg 1$ implies weakly

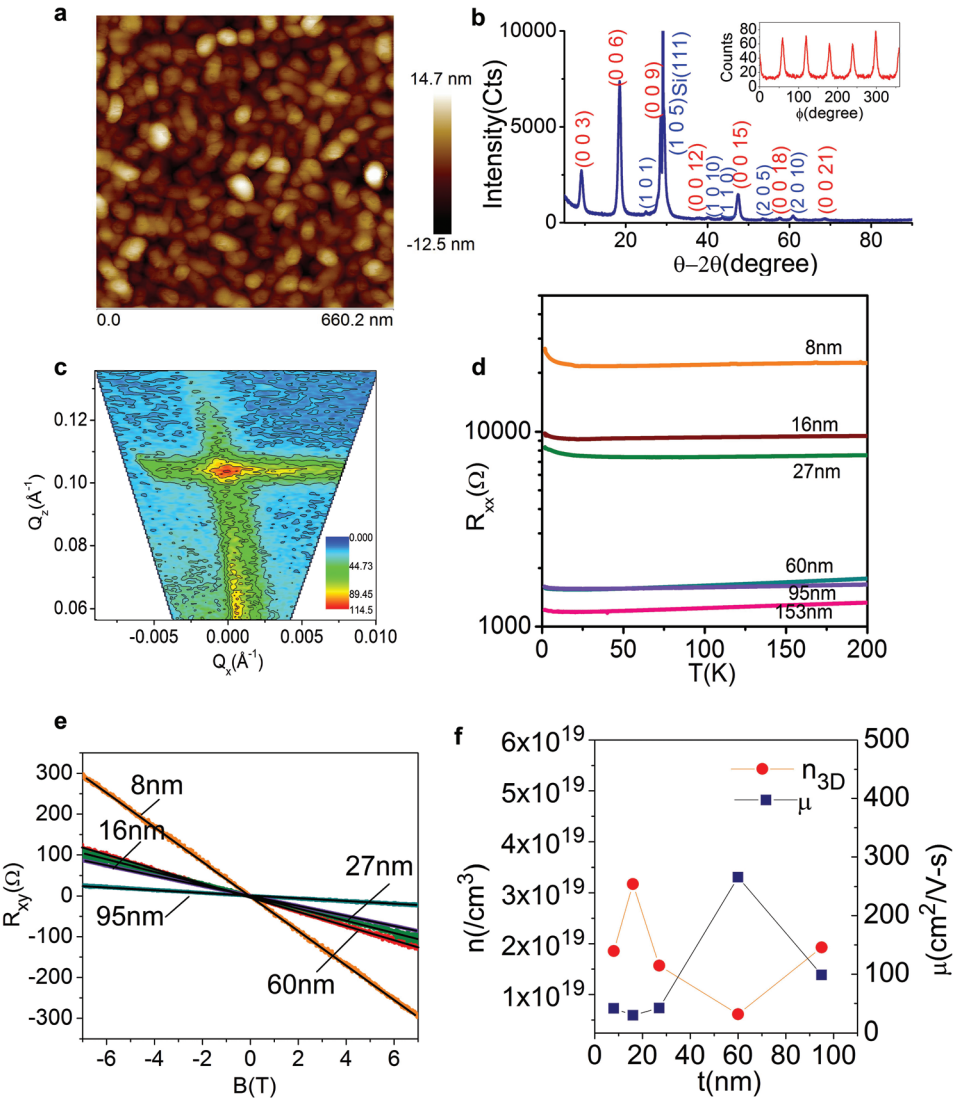

Fig. 3 (a) AFM image showing the surface topography of a thin film sample of Tl nanocrystals. (b) Standard θ–2θ XRD scan of a thin film shows that (003) peaks (marked in red) are dominant, implying a preferential orientation in the *c*-axis direction. Non-oriented peaks (marked in blue) reflect the granularity of our samples. Inset: Azimuthal scan of (105) planes of Bi_2Se_3 shows a six-fold symmetry and a large FWHM ~8°. (c) Reciprocal space map of (003) peak. The peak broadening is used to estimate grain dimension. The sample thickness used for the AFM and XRD measurements is 16 nm. (d) *R*–*T* for granular samples with different thicknesses. (e) R_{xy} *vs.* *B* for samples with different thicknesses. (f) Hall mobility and carrier density extracted by performing a linear fit to Hall data. The error bars are smaller than the symbol sizes.

disordered conduction while $g = k_F l_e \ll 1$ implies strong localization, g being the dimensionless conductance. For our samples, $g \sim 2$–3 which puts our samples in a regime proximate to the localization transition. The small grain size limits the mean free path of electrons. While intra-grain transport remains diffusive, the proximity to localization is a consequence of limited inter-grain transport which proceeds through electron tunneling across barriers. At low temperatures, the probability of tunneling can be approximated as $1/\tau_{\text{inter-grain}} \sim e^{-\Delta/k_B T}$, where Δ is the charging energy associated with a single grain. At low temperatures $1/\tau_{\text{inter-grain}}$ is exponentially suppressed giving rise to an insulating upturn in resistivity. While it is common to observe such a resistivity upturn in topological insulator samples due to electron–electron interactions,[21,22,28] we have used a fitting based on eqn (8) in ref. 28 and have found that the upturn we observe is too large to be explained as a consequence of electron–electron interactions alone.

We now seek evidence for surface state transport. A strong manifestation of the topological properties of surface states obeying the Dirac equation is the Berry phase of π due to the helical spin structure of electrons.[4,29] An elegant method to estimate the Berry phase of electrons is to study the quantum oscillations of sample resistance in a magnetic field. However, the low carrier mobility (Fig. 3(f)) in our samples due to their intrinsic granular nature precludes the observation of quantum oscillations in realistic magnetic fields. Instead, we turn to another effect where the Berry phase plays a dominant

role, namely weak antilocalization (WAL) in magnetoconductance (MC) measurements. The intrinsic Berry phase of π associated with the chiral carriers results in a destructive interference of electronic trajectories that begin and end at the same point in space. This essentially leads to a suppression of back-scattering. However, when a magnetic field is applied, time reversal symmetry is continuously broken and electrons acquire an additional Aharonov–Bohm phase that eventually destroys this effect, resulting in a steady increase of sample resistance with increasing magnetic field. This effect has been widely used to study the properties of topological insulators, especially to determine sample parameters like the number of coherent electronic channels that participate in current conduction and the electronic phase coherence length.[30–36] All our samples show WAL behavior[26] (Fig. 4(a and b)) both in perpendicular and parallel magnetic fields. The conductivity corrections from perpendicular WAL are described by using the Hikami–Larkin–Nagaoka (HLN) formula[37,38] in the form derived for topological insulators:[39,40]

$$\Delta\sigma_{\perp}(B_{\perp}) = -\alpha_{\perp}\frac{e^2}{2\pi^2\hbar} \times\left[\psi\left(\frac{1}{2}+\frac{\hbar}{4el_{\phi}^2B_{\perp}}\right)-\ln\left(\frac{\hbar}{4el_{\phi}^2B_{\perp}}\right)\right] \quad (9)$$

in the limit of strong spin–orbit scattering, where σ is the sample conductivity, $B_{\perp}$ is the applied magnetic field, l_{φ} is the phase coherence length, and $\psi(x)$ denotes the digamma function. The prefactor $\alpha_{\perp}$ determines the number of independent electronic channels that contribute to conductance corrections, with a value of 0.5 for each such channel.

WAL in a parallel magnetic field[41,42] is sensitive not only to the Berry phase but also to the vertical motion of electrons, therefore providing additional information about the spatial distribution of electronic channels. This was first realized by Altshuler and Aronov[43] and later extended to obtain the following general formula:[43–45]

$$\Delta\sigma_{\parallel}(B_{\parallel}) = -\alpha_{\parallel}\frac{e^2}{2\pi^2\hbar}\ln(1+{B_{\parallel}}^2/{B_{\phi}}^2), \quad (10)$$

where $B_{\phi} = \hbar/(e\lambda^* l_{\phi})$. Here we treat λ^* as a fitting parameter and discuss its implications later.

Our experimental data fit remarkably well to these formula to a large range of magnetic field (7 T) and temperature (2 K–30 K) (see ESI, Fig. S3† for details of fitting for every measured sample at different temperatures and magnetic field configurations). The results of our fitting are shown in Fig. 4(c)–(e). In the thick film regime, $\alpha_{\perp/\parallel} \simeq 1$ in all ranges of temperature. More strikingly, the match between $\alpha_{\perp}$ and $\alpha_{\parallel}$ suggests that in both field configurations, the same channels contribute to WAL. Additionally $\alpha_{\perp/\parallel} \simeq 1$ indicates that both parallel and perpendicular magnetic fields interact with the same two transport channels. In the thin film regime, perpendicular and in-plane field measurements yield similar values of α, but with $\alpha_{\perp/\parallel} \simeq 0.5$ indicating a single transport channel.

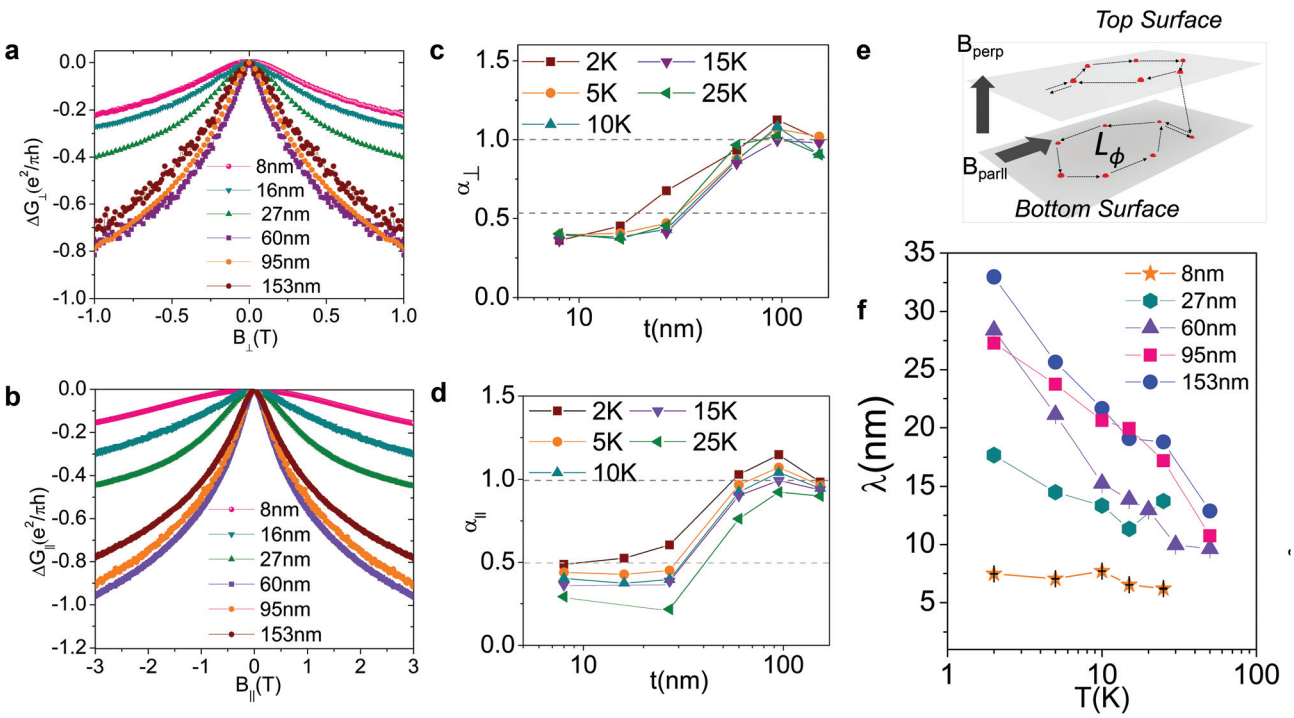

Fig. 4 Thickness dependence of magnetoconductance for (a) perpendicular and (b) parallel magnetic fields (symmetrized). (c) $\alpha_{\perp}$ and (d) $\alpha_{\parallel}$ extracted from WAL analysis indicating decoupling of surface states with increasing sample thickness. (e) Mechanism of WAL due to suppressed back-scattering. (f) Surface state penetration depth λ for different sample thicknesses and temperatures. Error bars, wherever not shown, are smaller than the symbol sizes.

Let us understand what these channels can correspond to. In a conventional disordered metallic system without any topological properties, one expects $|\alpha_{\perp/\|}| = 0.5$ for all ranges of sample thickness. On the contrary, we observe a distinct cross-over of $\alpha_{\perp/\|}$ from 0.5 to 1 indicating that the number of channels increases by 1 above a sample thickness of $t \approx 60$ nm (Fig. 4(c and d)). This clearly indicates that our samples do not behave as conventional metallic conductors with spin–orbit disorder. Having ruled out the possibility that our samples behave as topologically trivial conductors, we try to examine the various ways in which a combination of bulk states and a pair of topological surface states could give rise to our observations. Here, we have three possibilities to consider: the magnetoresistance signatures arise (i) from bulk states alone (ii) from a combination of bulk states and surface states, and (iii) from surface states alone. The first possibility may be easily ruled out: it is clear that if only bulk states contributed to WAL, there would be no cross-over of $\alpha_{\perp/\|}$ from 0.5 to 1. In fact, we would have obtained $\alpha_\perp = \alpha_\| = 0.5$ regardless of the sample thickness. Considering possibility (ii), we argue that if the WAL effect indeed arose from a combination of bulk and surface states, we would have obtained signatures that are in complete contradiction with our experimental observations. First, for WAL measured in perpendicular magnetic fields, we should have observed a cross-over from $\alpha_\perp = 0.5$ for thin films where all channels are coupled to $\alpha_\perp = 1.5$ in the thick film limit, when the bulk and the two surface states contributed to WAL as three independent channels. However, we do not observe $\alpha_\perp > 1$ even for the sample with a thickness of 153 nm. Second, if bulk states contributed significantly to the WAL effect, we would have obtained drastically different results from the parallel magnetic field MR measurements. When a magnetic field is applied parallel to the plane of the sample, the bulk states interact more strongly with the magnetic field compared to the surface states which are expected to show comparatively smaller areas of cross-section, especially in thicker samples. Therefore, a sizeable contribution from the bulk states would give rise to $\alpha_\| = 0.5$, especially for thick samples where the bulk contribution would be large. Yet, our measurements show that $\alpha_\|$ also shows a cross-over from 0.5 to 1.0 with increasing sample thickness. If the WAL signatures were dominated by bulk states, such a cross-over cannot be expected.

On the other hand, possibility (iii), that is, WAL dominated completely by surface states, can coherently explain our experimental results. Existing WAL studies on TIs suggest that the cross-over of $\alpha_{\perp/\|}$ from 0.5 to 1.0 is a robust signature of the presence of a pair of topological surface states.[35,46,47] In fact, the absence of a contribution from the bulk states explains the fact that the values of $\alpha_\perp$ and $\alpha_\|$ and their cross-overs match over the entire range of sample thickness and temperature. The surface states have a finite penetration depth λ into the bulk of the material. In ideal TIs, it is expected that $\alpha_{\perp/\|} = 0.5$ when $t < 2\lambda$ and 1.0 when $t > 2\lambda$, where $t = 2\lambda$ is the thickness where the surface states just begin to overlap. This cross-over is exactly what is observed in our system, and has been previously observed only in high quality bulk insulating TIs like Cu doped Bi_2Se_3,[35] while samples with more bulk conduction invariably fail to demonstrate the cross-over to $\alpha_\perp = 1$ (ref. 34 and 36) unless the bulk carrier densities are suppressed by other means like electrostatic gating or chemical counter-doping.[48] While this cross-over points to a pair of decoupled TSS, the cross-over thickness in previous experiments does not agree with theory. For example, in the experiments by Brahlek *et al.*,[35] the cross-over thickness was $t \sim 20$ nm even though the surface state penetration depth was only $\lambda \sim 1$–2 nm in their samples.

To investigate this further we need to accurately estimate the surface state penetration depth in our samples. We focus on the behavior of λ^* extracted from the parallel field WAL. In the conventional Altshuler–Aronov theory[43] for parallel field WAL in 2D electron systems, $\lambda^* = \sqrt{\beta}t$, where t is the sample thickness and β is a numerical factor of order unity that is determined by the disorder in the sample and remains independent of temperature. However, our experiments present a completely different picture. As shown in Fig. 4(f), λ^* extracted from our measurements does not scale linearly with the sample thickness. Additionally, it shows a strong temperature dependence for thicker samples. On the other hand, it has recently been pointed out[49,50] that in the case of ideal TIs, the interaction of the magnetic field is limited to electrons confined only along the top and bottom surfaces of the sample, and therefore λ^* may directly correspond to the surface state penetration depth λ. In fact, Lin *et al.*[51] found that the λ^* measured in their TI thin films showed a strong temperature dependence apart from other departures from conventional theoretical models.[43–45] If λ is taken to be the surface state penetration depth as suggested by this model,[49,50] a consistent picture emerges as we describe below. We comment here that this model relies only on two properties of TIs: the finite penetration depth of surface states and the Dirac dispersion governing their dynamics. Therefore, even though this model was originally envisaged for crystalline TIs, it is more general and can even be applied to complicated TI systems such as ours. In this scenario, λ^* becomes exactly equal to the surface state penetration depth λ.

The consistency of this interpretation is remarkable: in the thin film limit, where surface states exist throughout the volume of the film, the values of λ match remarkably well with the thickness of the film in the entire temperature range. In the thick film limit however, $\lambda \approx 30$ nm at 2 K for all the samples. This is exactly half the sample thickness $t \approx 60$ nm for which we observe a coupling/decoupling transition in α. The unusually large penetration depth allows the surface states to interact even with a parallel magnetic field and gives an unexpectedly large parallel field MR. The fact that λ is not only larger than the typical surface state penetration depth (1–2 nm) found in single crystal TIs, but is also much larger than the vertical grain size ($L \sim 2$–3 nm) indicates the remarkable macroscopic nature of this TI phase and its surface states as predicted by our theoretical model. More importantly, the fact that the cross-over of α happens almost exactly when the sample thickness $t \sim 2\lambda$ demonstrates that our granular TIs display ideal TI behavior.

It therefore comes as a surprise that our samples with bulk carrier concentrations $n \approx 10^{19}$ cm^{-3} show not only a distinct cross-over in α, but also that the cross-over is exactly at the expected sample thickness. This is a consequence of the highly granular nature of our samples that makes the bulk electronic states virtually localized within individual granules as demonstrated by their close proximity to the strong localization limit ($g \sim 2$–3). In such a disordered bulk, electrical conduction is not purely diffusive but proceeds through a combination of carrier diffusion and inter-grain hopping as discussed before. Such localized states cannot strongly contribute to weak (anti)localization effects which is a feature of quantum interference of carriers diffusing through a weakly disordered landscape. The highly granular nature of the bulk of our samples prohibits such a free diffusion of bulk carriers and causes quantum corrections to conductance from weak (anti) localization effects to either disappear or decrease substantially in magnitude. In fact, theoretical studies of highly disordered conductors show that weak (anti)localization effects could still arise, albeit with a much smaller amplitude.[52,53] In fact, the parameter α gets significantly reduced to $\alpha = \frac{1}{2} - 1/(\pi g)$ where g is the dimensionless conductance described before. Moreover, this theoretical estimate assumes that $g \simeq 1$ and that the disorder strength can be treated perturbatively. Given that the estimates of $g \sim 2$–3 in our granular samples represent a combination of the bulk as well as the surface carriers, the bulk states may well have significantly lower values of g than what we estimate, in which case α may actually turn out to be zero.

On the other hand, a defining characteristic of surface states in strong topological insulators is that they are immune to strong localization. In fact, rather counter-intuitively, it has been theoretically shown that strong disorder can drive such systems deeper into a topological phase[20,54] with robust surface state transport even when the bulk is Anderson localized. Recent experimental studies on highly disordered topological insulators[53,55] confirm this picture. In fact, Liao *et al.*[53] studied ultra-thin films (2 nm–5 nm) of topological insulators where they observed a robust WAL effect with $\alpha \sim 0.5$, even when their samples were driven into the strong localization regime ($g \ll 1$). Since these films were ultra-thin (2 nm–5 nm), only (coupled) surface states were expected to contribute to transport. These experiments indicate the remarkable resilience of surface states to strong localization, and the persistence of the WAL effect of the surface states up to very large disorder strengths. Therefore, even though our samples are highly granular, the surface states are immune to localization and give rise to robust WAL with $\alpha = 0.5$ per surface state. On the other hand, such a mechanism of "topological protection" is absent for the bulk states which easily localize and either do not contribute to the WAL effect, or contribute with a substantially reduced value of α such that their feeble magnetoconductance signatures are completely overshadowed by the WAL signatures arising out of the surface states. This is a remarkable consequence of bulk topology that has been theoretically predicted in strongly disordered systems like topological Anderson insulators,[20,54] but has never been realized before experimentally.

While the emergence of the TI phase indicates that $t_1 < t_2$ in our samples, it is the experimental value of t_1/t_2 that determines the properties of the surface states (Fig. 4(f)). This manifests as an unusually large λ and its remarkable temperature dependence. For the thickest film, λ varies from about 33 nm at 2 K to 12 nm at 50 K. From the expression for the surface state penetration depth $\lambda = L/\log(t_2/t_1)$, we estimate that t_1/t_2 varies from 0.85 to 0.94 for $L = 2$ nm. This increase of t_2 with temperature is expected due to the activated nature of tunneling across potential barriers. The fact that $t_1/t_2 \sim 1$ indicates that our samples are close to a topological phase transition and that the system surprisingly goes deeper into the topological phase with increasing temperature. In fact, this shows that temperature can be used as a control for 'topology' in our system, suggesting a more fundamental approach where the ratio t_1/t_2 can be engineered to fabricate 'designer TIs' as envisaged in several theoretical studies.[14,16,17]

4. Discussion

Apart from their technological ramifications, granular TIs also offer interesting possibilities in terms of investigating the fundamental physics governing TIs. Our demonstrations of robust topological surface states and large surface state penetration depths show that granular TIs form an interesting test bed for studying Dirac fermion physics. Unlike crystalline TIs, where the SOC in the bulk alone determines the scale of band inversion, in granular TIs this is not the case. While SOC is indeed a necessary ingredient in granular TIs, it is not sufficient to drive a bulk gap inversion. Instead, it is the ratio of the coupling strengths t_1/t_2 that ultimately determines whether the overall system behaves as a TI or not. Our work further shows that this criterion needs to be satisfied only on an average since modest disorder which causes grain to grain variations in t_1 and t_2 does not affect the overall results. This is highly reminiscent of the physics of topological Anderson insulators[20] and aperiodic topological insulators, although the microscopic mechanisms are quite different. From a practical point of view, this becomes very relevant. While it is possible to control the bulk SOC in crystalline TIs by doping, granular TI samples are much easier to fabricate and do not rely on tuning the bulk SOC. The complex interplay of band structures, doping concentrations and other physical parameters that arise due to heavy bulk doping can therefore be completely sidestepped.

In summary, we have shown that an assembly of TI nanocrystals can emerge as a macroscopic TI with tunable properties. We observe decoupled topological surface states localized at the top and bottom surfaces of our granular thin films with unusually large penetration depths. Further, their properties can be tuned by altering the ratio of inter-grain to intra-grain tunneling, which manifests as a temperature dependent parameter in our experiments. Future experimental

and theoretical work can focus on careful tuning of this ratio to study topological phase transitions, the unique properties of such model TI systems, and the diverse electronics applications employing their topological tunability.

Acknowledgements

A.B. and O.D. thank MHRD, Govt. of India for financial support. K. M. thanks CSIR, India for financial support. D. S. thanks DST, India for support under Grant No. SR/S2/JCB-44/2010. P. S. A. K. acknowledges Nanomission, DST, Govt. of India for support.

References

1 M. Z. Hasan and C. L. Kane, *Rev. Mod. Phys.*, 2010, **82**, 3045.
2 X.-L. Qi and S.-C. Zhang, *Rev. Mod. Phys.*, 2011, **83**, 1057.
3 Y. L. Chen, J. G. Analytis, J.-H. Chu, Z. K. Liu, S.-K. Mo, X.-L. Qi, H. J. Zhang, D. H. Lu, X. Dai, Z. Fang, *et al.*, *Science*, 2009, **325**, 178.
4 Y. Xia, D. Qian, D. Hsieh, L. Wray, A. Pal, H. Lin, A. Bansil, D. Grauer, Y. S. Hor, R. J. Cava, *et al.*, *Nat. Phys.*, 2009, **5**, 398.
5 D. Hsieh, Y. Xia, D. Qian, L. Wray, J. H. Dil, F. Meier, J. Osterwalder, L. Patthey, J. G. Checkelsky, N. P. Ong, A. V. Fedorov, H. Lin, A. Bansil, D. Grauer, Y. S. Hor, R. J. Cava and M. Z. Hasan, *Nature*, 2009, **460**, 1101.
6 P. Roushan, J. Seo, C. V. Parker, Y. S. Hor, D. Hsieh, D. Qian, A. Richardella, M. Z. Hasan, R. J. Cava and A. Yazdani, *Nature*, 2009, **460**, 1106.
7 C. Li, O. vant Erve, J. Robinson, Y. Liu, L. Li and B. Jonker, *Nat. Nanotechnol.*, 2014, **9**, 218–224.
8 C.-Z. Chang, J. Zhang, X. Feng, J. Shen, Z. Zhang, M. Guo, K. Li, Y. Ou, P. Wei, L.-L. Wang, *et al.*, *Science*, 2013, **340**, 167–170.
9 H.-H. Sun, K.-W. Zhang, L.-H. Hu, C. Li, G.-Y. Wang, H.-Y. Ma, Z.-A. Xu, C.-L. Gao, D.-D. Guan, Y.-Y. Li, *et al.*, *Phys. Rev. Lett.*, 2016, **116**, 257003.
10 Y. Xu, I. Miotkowski, C. Liu, J. Tian, H. Nam, N. Alidoust, J. Hu, C.-K. Shih, M. Z. Hasan and Y. P. Chen, *Nat. Phys.*, 2014, **10**, 956–963.
11 Z. H. Wang, L. Yang, X. J. Li, X. T. Zhao, H. L. Wang, Z. D. Zhang and X. P. A. Gao, *Nano Lett.*, 2014, **14**, 6510.
12 P. Olbrich, L. E. Golub, T. Herrmann, S. N. Danilov, H. Plank, V. V. Belkov, G. Mussler, C. Weyrich, C. M. Schneider, J. Kampmeier, *et al.*, *Phys. Rev. Lett.*, 2014, **113**, 096601.
13 H. Zhang, J. Yao, J. Shao, H. Li, S. Li, D. Bao, C. Wang and G. Yang, *Sci. Rep.*, 2014, **4**, 5876.
14 A. A. Burkov and L. Balents, *Phys. Rev. Lett.*, 2011, **107**, 127205.
15 J. Kim, J. Kim, K.-S. Kim and S.-H. Jhi, *Phys. Rev. Lett.*, 2012, **109**, 146601.
16 T. Das and A. V. Balatsky, *Nat. Commun.*, 2013, **4**, 1972.
17 X. Li, F. Zhang, Q. Niu and J. Feng, *Sci. Rep.*, 2014, **4**, 6397.
18 T. H. Hsieh, H. Ishizuka, L. Balents and T. L. Hughes, *Phys. Rev. Lett.*, 2016, **116**, 086802.
19 M. Dzero, K. Sun, V. Galitski and P. Coleman, *Phys. Rev. Lett.*, 2010, **104**, 106408.
20 J. Li, R.-L. Chu, J. K. Jain and S.-Q. Shen, *Phys. Rev. Lett.*, 2009, **102**, 136806.
21 Y. Zhao, H. Liu, X. Guo, Y. Jiang, Y. Sun, H. Wang, Y. Wang, H.-D. Li, M.-H. Xie, X.-C. Xie, *et al.*, *Nano Lett.*, 2014, **14**, 5244–5249.
22 Y. Zhao, C.-Z. Chang, Y. Jiang, A. DaSilva, Y. Sun, H. Wang, Y. Xing, Y. Wang, K. He, X. Ma, *et al.*, *Sci. Rep.*, 2013, **3**, 3060.
23 F. Zhang, C. L. Kane and E. J. Mele, *Phys. Rev. B: Condens. Matter*, 2012, **86**, 081303.
24 O. Deb, A. Soori and D. Sen, *J. Phys.: Condens. Matter*, 2014, **26**, 315009.
25 R. D'Agosta, G. Vignale and R. Raimondi, *Phys. Rev. Lett.*, 2005, **94**, 086801.
26 ESI,† 2017.
27 I. S. Beloborodov, A. V. Lopatin, V. M. Vinokur and K. B. Efetov, *Rev. Mod. Phys.*, 2007, **79**, 469.
28 J. Wang, A. M. DaSilva, C.-Z. Chang, K. He, J. Jain, N. Samarth, X.-C. Ma, Q.-K. Xue and M. H. Chan, *Phys. Rev. B: Condens. Matter*, 2011, **83**, 245438.
29 L. Fu and C. L. Kane, *Phys. Rev. B: Condens. Matter*, 2007, **76**, 045302.
30 J. Chen, H. Qin, F. Yang, J. Liu, T. Guan, F. Qu, G. Zhang, J. Shi, X. Xie, C. Yang, *et al.*, *Phys. Rev. Lett.*, 2010, **105**, 176602.
31 J. Checkelsky, Y. Hor, R. Cava and N. Ong, *Phys. Rev. Lett.*, 2011, **106**, 196801.
32 J. Chen, X. He, K. Wu, Z. Ji, L. Lu, J. Shi, J. Smet and Y. Li, *Phys. Rev. B: Condens. Matter*, 2011, **83**, 241304.
33 J. J. Cha, D. Kong, S.-S. Hong, J. G. Analytis, K. Lai and Y. Cui, *Nano Lett.*, 2012, **12**, 1107.
34 A. A. Taskin, S. Sasaki, K. Segawa and Y. Ando, *Phys. Rev. Lett.*, 2012, **109**, 066803.
35 M. Brahlek, N. Koirala, M. Salehi, N. Bansal and S. Oh, *Phys. Rev. Lett.*, 2014, **113**, 026801.
36 N. Bansal, Y. S. Kim, M. Brahlek, E. Edrey and S. Oh, *Phys. Rev. Lett.*, 2012, **109**, 116804.
37 S. Hikami, A. I. Larkin and Y. Nagaoka, *Prog. Theor. Phys.*, 1980, **63**, 707.
38 B. L. Altshuler, D. Khmel'Nitzkii, A. I. Larkin and P. A. Lee, *Phys. Rev. B: Condens. Matter*, 1980, **22**, 5142.
39 I. Garate and L. Glazman, *Phys. Rev. B: Condens. Matter*, 2012, **86**, 035422.
40 H.-Z. Lu, J. Shi and S.-Q. Shen, *Phys. Rev. Lett.*, 2011, **107**, 076801.
41 H. Wang, H. Liu, C.-Z. Chang, H. Zuo, Y. Zhao, Y. Sun, Z. Xia, K. He, X. Ma, X. Xie, *et al.*, *Sci. Rep.*, 2014, **4**, 5817.
42 C. Lin, X. He, J. Liao, X. Wang, V. Sacksteder IV, W. Yang, T. Guan, Q. Zhang, L. Gu, G. Zhang, *et al.*, *Phys. Rev. B: Condens. Matter*, 2013, **88**, 041307.
43 B. Al'tshuler and A. Aronov, *JETP Lett.*, 1981, **33**, 499.
44 V. Dugaev and D. Khmel'nitskii, *Zh. Eksp. Teor. Fiz.*, 1984, **86**, 1784.

45 C. W. J. Beenakker and H. van Houten, *Phys. Rev. B: Condens. Matter*, 1988, **38**, 3232.
46 H. Steinberg, J.-B. Laloë, V. Fatemi, J. S. Moodera and P. Jarillo-Herrero, *Phys. Rev. B: Condens. Matter*, 2011, **84**, 233101.
47 D. Kim, P. Syers, N. P. Butch, J. Paglione and M. S. Fuhrer, *Nat. Commun.*, 2013, **4**, 2040.
48 A. Banerjee, A. Sundaresh, K. Majhi, R. Ganesan and P. Anil Kumar, *Appl. Phys. Lett.*, 2016, **109**, 232408.
49 G. Tkachov and E. M. Hankiewicz, *Phys. Rev. B: Condens. Matter*, 2011, **84**, 035444.
50 V. E. Sacksteder IV, K. B. Arnardottir, S. Kettemann and I. A. Shelykh, *Phys. Rev. B: Condens. Matter*, 2014, **90**, 235148.
51 C. J. Lin, X. Y. He, J. Liao, X. X. Wang, V. Sacksteder IV, W. M. Yang, T. Guan, Q. M. Zhang, L. Gu, G. Y. Zhang, *et al.*, *Phys. Rev. B: Condens. Matter*, 2013, **88**, 041307.
52 G. Minkov, A. Germanenko and I. Gornyi, *Phys. Rev. B: Condens. Matter*, 2004, **70**, 245423.
53 J. Liao, Y. Ou, X. Feng, S. Yang, C. Lin, W. Yang, K. Wu, K. He, X. Ma, Q.-K. Xue, *et al.*, *Phys. Rev. Lett.*, 2015, **114**, 216601.
54 H.-M. Guo, G. Rosenberg, G. Refael and M. Franz, *Phys. Rev. Lett.*, 2010, **105**, 216601.
55 R. Du, H.-C. Hsu, A. C. Balram, Y. Yin, S. Dong, W. Dai, W. Zhao, D. Kim, S.-Y. Yu, J. Wang, *et al.*, *Phys. Rev. B: Condens. Matter*, 2016, **93**, 195402.